Experimental Measurements of Ion Heating in Collisional Plasma Shocks and Interpenetrating Supersonic Plasma Flows

Samuel J. Langendorf,[1,*] Kevin C. Yates,[2,1] Scott C. Hsu,[1,†] Carsten Thoma,[3] and Mark Gilmore[2]
[1]*Los Alamos National Laboratory, Los Alamos, New Mexico 87545, USA*
[2]*University of New Mexico, Albuquerque, New Mexico 87131, USA*
[3]*Voss Scientific, Albuquerque, New Mexico 87108, USA*

(Received 21 May 2018; revised manuscript received 26 September 2018; published 31 October 2018)

We present time-resolved measurements of ion heating due to collisional plasma shocks and interpenetrating supersonic plasma flows, which are formed by the oblique merging of two coaxial-gun-formed plasma jets. Our study is repeated using four jet species: N, Ar, Kr, and Xe. In conditions with small interpenetration between jets, the observed peak ion temperature T_i is consistent with the predictions of collisional plasma-shock theory showing a substantial elevation of T_i above the electron temperature T_e and also the subsequent decrease of T_i on the classical ion-electron temperature-equilibration timescale. In conditions of significant interpenetration between jets, such that shocks do not apparently form, the observed peak T_i is still appreciable and greater than T_e but much lower than that predicted by collisional plasma-shock theory. Experimental results are compared with multifluid plasma simulations.

DOI: 10.1103/PhysRevLett.121.185001

Shocks are a fundamental feature of supersonic plasma flows and affect the energy balance and dynamical evolution of physical systems in which the shocks are embedded, e.g., in astrophysical systems [1–4] or in high-energy-density (HED) [5] and inertial-confinement-fusion (ICF) [6] experiments. Differing in two key respects from hydrodynamic shocks, plasma shocks (1) are mediated either by classical Coulomb collisions between plasma particles (collisional plasma shock [7,8]) or by collective effects such as the Weibel instability [9–11] (collisionless plasma shock [12]), and (2) they are more complex due to the coupled interactions of electrons, ions (sometimes multiple species), electromagnetic fields, and radiative and equation-of-state (EOS) effects. This Letter focuses on ion heating in unmagnetized collisional plasma shocks and interpenetrating supersonic plasma flows, where radiative and thermal losses and EOS effects are important. Related recent experiments include colliding railgun plasma jets [13–15], wire-array Z pinches [16–18], and laser ablation of solid targets [19]. The latter is also used to study collisionless shocks [20–24]. The study of interpenetrating, colliding plasma flows has a long history, e.g., Refs. [25–27]. Time-resolved ion-temperature data were not reported in nor were they the focus of the prior works.

This Letter presents the first detailed diagnostic study of the time evolution of ion temperature T_i and ion heating due to unmagnetized collisional plasma shocks and interpenetrating supersonic plasma flows, with sufficient detail to compare with theory and simulation across species and collisionality regimes. These new fundamental data are valuable for validating and improving first-principles modeling of these phenomena, e.g., Refs. [28–30], which are crucial for advancements in modeling HED and ICF experiments and a range of astrophysical plasmas. There are significant disagreements among different codes and models [31,32], possibly due to specific choices of collisionality, transport, and EOS models and/or their implementations. Although HED and ICF experiments have different absolute plasma parameters, our experiments are in a similar regime with respect to collisionality and EOS, such that the same models and codes are applicable.

The results presented here were obtained on and motivated by the Plasma Liner Experiment (PLX) [33,34], where six coaxial plasma guns [34,35] are mounted on a 2.74-m-diameter spherical vacuum chamber. In these experiments, two plasma jets are fired with merging half angle $\theta = 11.6°$ or 20.5°, as shown in Figs. 1(a) and 1(b), respectively. At the gun nozzle, each jet has ion density $n_i \sim 2 \times 10^{16}$ cm^{-3}, electron temperature $T_e \approx T_i \approx 1.5$ eV, mean charge $\bar{Z} \approx 1$, diameter $\approx$ 8.5 cm, and speed $v_{\rm jet} \approx 25$–80 km/s [34]. Details of the gun design and jet characterization are reported elsewhere [34,35]. Extensive prior work [13,14,36] showed that a jet propagating over ∼1 m expands radially and axially at approximately the internal sound speed C_s, T_e and $v_{\rm jet}$ stay approximately constant, n_i decreases consistently with mass conservation, magnetic field strength decays by $1/e$ every few μs such that both the thermal pressure and kinetic energy density (of the jet directed motion) dominate over the magnetic pressure when the jets merge, and that density jumps and jet-merging morphology are consistent with oblique collisional shock formation.

The plasma parameters reported in this work, i.e., T_i, T_e, electron density n_e, $\bar{Z}$, and $v_{\rm jet}$, are inferred from diagnostic measurements (positions shown in Fig. 1). Plasma T_i is

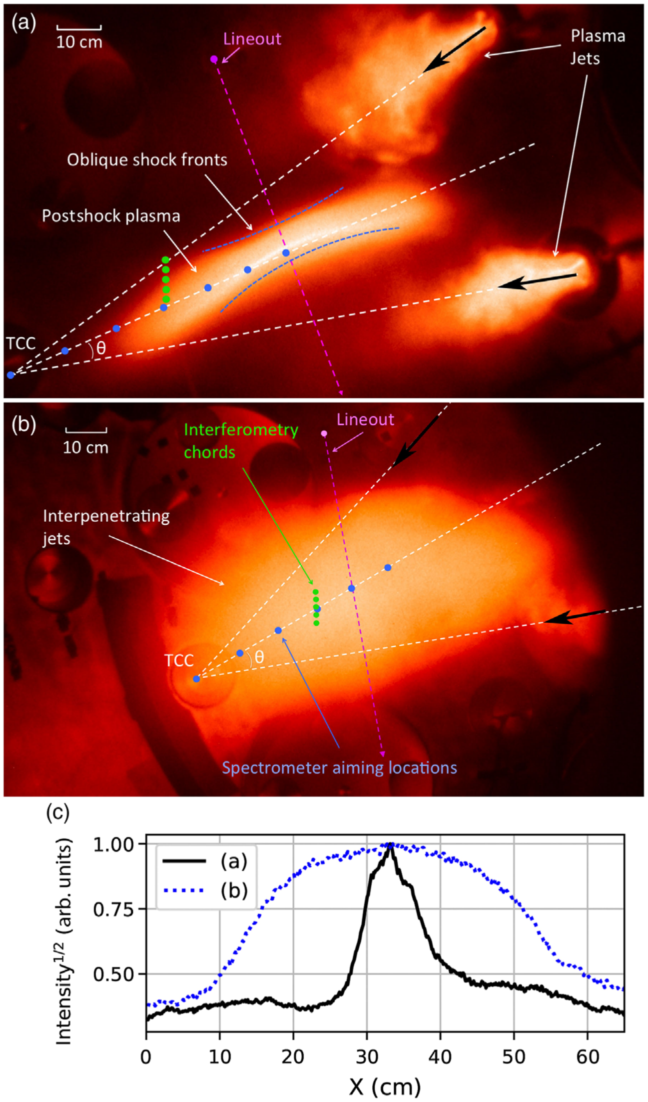

FIG. 1. Fast-camera, visible-light images (10-ns exposure, log intensity, false color) of two merging Ar plasma jets (black arrows indicate direction of travel) with (a) $\theta = 11.6°$ (shot 2559, $t = 38$ μs), showing the formation of oblique, collisional plasma shocks, and (b) $\theta = 20.5°$ (shot 1570, $t = 36$ μs), showing Ar jet-jet interpenetration (large region of diffuse emission) without apparent shock formation. Diagnostic chord positions (green and blue dots) and target-chamber center (TCC) are shown. (c) Lineouts of the square root of intensity correspond to the magenta dotted lines in (a) and (b).

measured via Doppler broadening of plasma ion line emission using a high-resolution, 4-m McPherson monochromator (2062DP) with a 2400-mm^{-1} grating and an intensified charge-coupled-device (ICCD) detector. The spectral resolution is 1.5 pm/pixel at the typical visible wavelengths of interest, sufficient to resolve $T_i \gtrsim$ a few eV for Xe and correspondingly smaller values for lighter species. The high-resolution spectrometer records two chords at a time with typical waist diameter of 2 cm; chord positions are indicated by the blue dots (10-cm separation) in Fig. 1. Doppler broadening is the primary source of line broadening in our parameter regime (the density is too low for Stark broadening to be appreciable), and the effects of differing Doppler shifts of different jets are minimized by viewing the merging at ≈90° relative to the directions of jet propagation. Turbulent motion of the merged plasma is not indicated in the experimental images. Line-integrated measurements of n_e are obtained using a multichord laser interferometer [37]. The density of the postshock or jet-interpenetration regions is measured using five interferometry chords (0.3-cm chord diameter and 1.5-cm spacing between chords) 30 cm from TCC, as shown by the green dots in Fig. 1. Plasma T_e and $\bar{Z}$ are bounded [36] by comparing broadband visible spectroscopy data [34] obtained along the same chord positions to atomic modeling using the inferred n_e from interferometry. Jet speeds are measured via a photodiode array at the end of each gun [34]. An ICCD camera (PCO dicam pro) obtains visible-light images of the shock formation or jet interpenetration. Further details of the PLX facility, coaxial plasma guns, diagnostics, and plasma-jet parameters are described in Ref. [34].

Figures 1(a) and 1(b) show fast-camera images of two jets merging with $\theta = 11.6°$ and 20.5°, respectively, and Fig. 1(c) shows lineouts of the square root of intensity across the region of jet merging. If T_e is nearly spatially uniform, which is consistent with both collisional plasma-shock theory [8] and our experimental measurements, then the lineouts in Fig. 1(c) are representative of the n_i profile. For the black curve, the gradient scale length of ∼ few cm is consistent with expected oblique collisional plasma-shock thicknesses (discussed later).

Figure 2(a) shows representative interferometry profiles of line-integrated n_e in the postmerged plasma. These measurements show small spatial variations in the postmerge region and are used to infer postmerge n_e. Figure 2(b) shows the broadband emission spectrum compared to PRISMSPECT modeling [38], which we use to bound T_e and $\bar{Z}$. The uncertainties in T_e and $\bar{Z}$ are determined based on the absence or presence of lines compared to PRISMSPECT modeling [36]. Postmerge values of n_e, T_e, and $\bar{Z}$ are summarized in Table I. Broadband spectra reveal that no impurity lines are observed during the first 10 μs of jet merging; the results in Table I are not expected to be significantly affected by impurities.

The primary result of this work is the measurement of the time evolution of T_i inferred from Doppler broadening of ionized emission lines in the postshock plasma or the region of jet-jet interpenetration as shown in Figs. 1(a) and 1(b), respectively. An example of the inference of T_i from Doppler spectroscopy data is shown in Fig. 3. Data at the earliest stage of jet merging show evidence of multiple overlapping line shapes (not shown here), which we believe to be due to interpenetration and systematic gun-angle-dependent Doppler shifts. These features are not observed

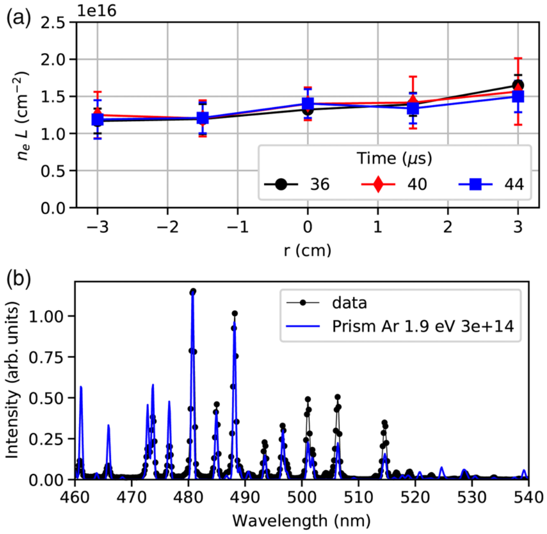

FIG. 2. (a) Example line-integrated electron density, at the three indicated times, of interpenetrating Ar plasma jets (shot 1579, $\theta = 20.5°$), as measured by interferometry [green dots in Fig. 1(b)], where $r < 0$ is below the midplane and error bars indicate $\pm 1\sigma$ of shot-to-shot variation. (b) Example visible spectral emission from merged plasma jets (shot 1579, $t = 38$ μs, 30 cm from TCC) and calculated spectra using PRISMSPECT [38] (uncertainty in T_e is ± 0.4 eV).

several μs later into the jet merging. In data processing, we reject multiple-line-shape cases and include only the cases that satisfy a threshold goodness of fit to a single Gaussian function.

Figure 4 shows inferred T_i vs time corresponding to cases (a)–(h) of Table I. Cases (a)–(c) and (g) are expected to be "collisional" with oblique shock formation [e.g., Fig. 1(a)], while cases (d)–(f) and (h) are expected to be "interpenetrating" without apparent shock formation [e.g., Fig. 1(b)]. Collisional and interpenetrating are defined in the next paragraph. Specific emission lines used were 463.0-nm N II, 480.6-nm Ar II, 473.9-nm Kr II, and 529.2-nm Xe II. In obtaining this data set at the positions indicated by the blue dots in Figs. 1(a) and 1(b), we recorded progressively later times as we moved the spectrometer viewing chords closer to TCC (over multiple shots) because the jets and merged plasma move from right to left in Figs. 1(a) and 1(b). All recorded data meeting the goodness-of-fit criterion are included in Fig. 4.

We consider the approximate interpenetration distance $L_{ii,s}$ between merging jets, which can vary from much smaller (collisional) to of the order or greater (interpenetrating) than the characteristic jet size $L \sim 20$ cm. Using average premerge jet parameters ($v_{\rm jet}$ from photodiodes, n_i decreased from measured postmerge $n_i = n_e/\bar{Z}$ by a factor of 2.5 for interpenetrating cases and 3.5 for shock-forming cases, which are approximations between theoretical limits of 2 and 4, respectively, for $\gamma = 5/3$, and $\bar{Z}$ inferred from spectroscopy), we estimate [39]

$$L_{ii,s} = \frac{v}{4\nu_{ii,s}} = \frac{v}{4}\left[9 \times 10^{-8} n_i \bar{Z}^4 \Lambda_{ii} \left(\frac{2}{\mu}\right) \frac{\mu^{1/2}}{\epsilon^{3/2}}\right]^{-1}, \quad (1)$$

where $v = 2v_{\rm jet}\sin\theta$ (cm/s) is the counterstreaming speed between the two jets, $\nu_{ii,s}$ the counterstreaming ion-ion slowing frequency in the fast limit ($\gg \nu_{ie,s}$ for our parameters), Λ_{ii} the Coulomb logarithm for counterstreaming ions in the presence of warm electrons [14,39], μ the ion-to-proton mass ratio, ϵ (eV) the energy associated with v, and the factor of 4 in the denominator accounts for the integral effect of slowing down [40]. For cases (a)–(c) and (g) of Table I, $L \gg L_{ii,s}$. For cases (d)–(f) and (h) of Table I, $L \lesssim L_{ii,s} \sim v\epsilon^{3/2} \sim v^4$.

If $L_{ii,s} \ll L$, the jets impact each other like pistons, and collisional plasma shocks typically form [13,14]. An upper

TABLE I. Summary of experimental parameters. The n_e, T_i, T_e, $\bar{Z}$, and ion-ion mean free path λ_i are average, postmerge values. The jet-jet interpenetration length $L_{ii,s}$ [see Eq. (1)], counterstreaming speed $v = 2v_{\rm jet}\sin\theta$, and jet Mach number $M = v/[\gamma k(T_i + \bar{Z}T_e)/m_i]^{1/2}$ are average, premerge values. The average $L_{ii,s}$ and λ_i values are not intended to be precise but to provide insight into the collisionality regime. The error ranges for $v_{\rm jet}$, v, n_e, and T_i are $\pm 1\sigma$ of the variation over multiple shots; those for T_e and $\bar{Z}$ represent uncertainties based on comparisons with PRISMSPECT spectral modeling.

Case	(a)	(b)	(c)	(d)	(e)	(f)	(g)	(h)
Half angle θ	11.6°	11.6°	11.6°	11.6°	20.5°	20.5°	20.5°	20.5°
Species	Ar	Xe	N	Kr	Ar	Xe	N	Kr
$v_{\rm jet}$ (km/s)	41.5 ± 4.5	24.3 ± 3.1	44.8 ± 4.6	64.8 ± 18.1	42.1 ± 4.8	27.4 ± 3.6	52.2 ± 3.5	57 ± 7.5
v (km/s)	16.7 ± 1.8	9.8 ± 1.2	18.1 ± 1.9	26.1 ± 7.3	29.4 ± 3.3	19.2 ± 2.5	36.5 ± 2.4	39.8 ± 5.3
n_e (10^{14} cm^{-3})	4.0 ± 0.5	4.8 ± 0.8	4.6 ± 0.4	3.8 ± 1.8	4.6 ± 1.0	13 ± 5.1	8.9 ± 1.4	11.6 ± 2.9
Peak T_i (eV)	18.1 ± 6.5	25.6 ± 3.2	10.2 ± 2.2	31.7 ± 21.3	32.0 ± 2.3	40.6 ± 10.0	16.6 ± 2.8	45.6 ± 10.4
T_e (eV)	2.0 ± 0.4	1.7 ± 0.4	1.7 ± 0.9	1.4 ± 0.6	2.0 ± 0.4	1.7 ± 0.4	2.6 ± 0.8	1.4 ± 0.6
$\bar{Z}$	1.0 ± 0.1	1.2 ± 0.2	1.0 ± 0.2	1.0 ± 0.2	1.0 ± 0.1	1.2 ± 0.2	1.1 ± 0.2	1.0 ± 0.2
$L_{ii,s}$ (cm)	2.5	1.5	0.2	56.2	26.6	10.2	4.0	190
λ_i (cm)	1.9	1.6	0.5	2.0	3.3	1.4	0.4	2.6
M	4.2	4.7	2.9	11.4	7.4	9.1	4.6	17.3

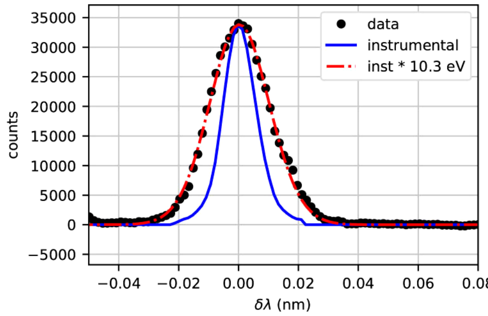

FIG. 3. Example of high-resolution spectroscopy data and fitting to infer $T_i = 10.3$ eV based on the best fit of the convolution of instrumental broadening with a Gaussian function (shot 1601, $t = 32\ \mu$s, 1-μs gate, $\theta = 11.6°$, Ar II 480.6-nm line, 30 cm from TCC, fitting error $= \pm 0.3$ eV).

bound for the jump in T_i across the shock, assuming that all of the heating goes to the ions, and T_e is uniform across the shock, is [41,42]

$$\frac{T_{i2}}{T_{i1}} = \left(1 + \frac{2(\gamma-1)}{(\gamma+1)^2}\frac{(\gamma M^2+1)}{M^2}(M^2-1)\right)(\alpha+1)-\alpha, \quad (2)$$

where subscripts "1" and "2" refer to pre- and postshock, respectively, $\gamma = 5/3$ is the polytropic index, preshock Mach number $M \equiv v/[\gamma k(T_i + \bar{Z}T_e)/m_i]^{1/2}$, $\alpha \equiv (\bar{Z}T_e)/T_{i1}$, and $T_{i1} = T_e$ is assumed. Predicted T_{i2} based on Eq. (2) are plotted as horizontal dotted lines in Fig. 4. Figure 4 shows that the measured peak T_i agrees well with Eq. (2) for shock-forming cases with $L_{ii,s} \ll L$ [Figs. 4(a)–4(c)], becomes increasingly smaller than predicted with increasing $L_{ii,s}$ [Figs. 4(a) and 4(g)], and is uniformly much smaller than predicted when $L_{ii,s} \gtrsim L$ [Figs. 4(d)–4(f) and 4(h)]. Within each species, the measured T_i evolution becomes less impulsive and has a broader temporal profile with increasing $L_{ii,s}$. When $L_{iis,s} \ll L$ [e.g., Fig. 1(a)], the estimated post-shock ion-ion mean free paths $\lambda_i \sim 1$ cm, consistent with the sharp jumps of the solid black curve of Fig. 1(c) being collisional shocks. When $L_{ii,s} \gtrsim L$, shocks do not appear to form [e.g., Fig. 1(b) and blue dotted curve of Fig. 1(c)].

The predicted, classical ion-electron temperature relaxation rate [39]

$$\frac{dT_i}{dt} = \left(1.8\times 10^{-19}\frac{(m_i m_e)^{1/2}\bar{Z}_i^2 n_e \Lambda_{ie}}{(m_i T_e + m_e T_i)^{3/2}}\right)(T_e - T_i) \quad (3)$$

is plotted in Fig. 4, overlaying the data. Agreement between the data and Eq. (3) is generally good. Discrepancies beyond the error bars motivate further detailed comparisons with theory or modeling, e.g., accounting for multidimensional, radiative, and EOS effects.

Finally, we perform 1D (counterstreaming component), multifluid calculations (Lagrangian particles advect electron and two ion-fluid quantities), including thermal or

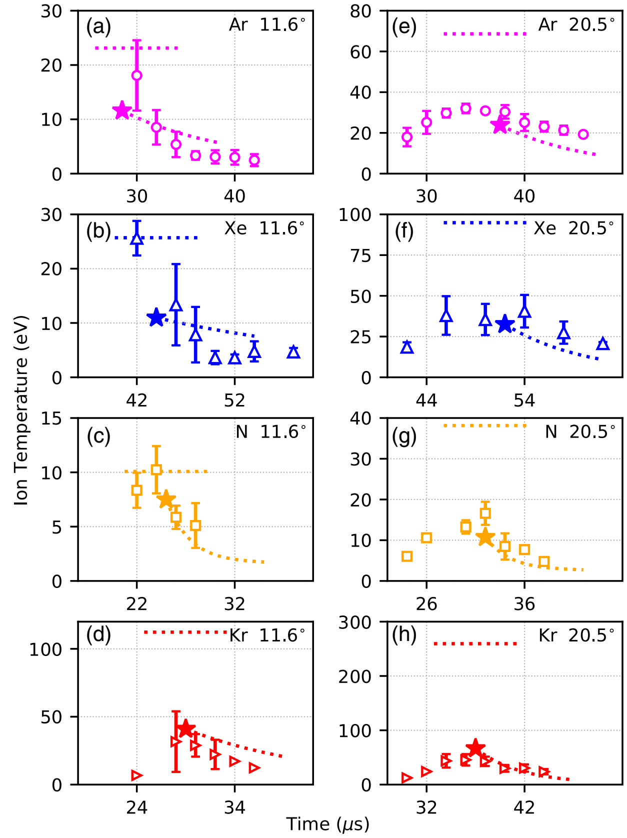

FIG. 4. Measured T_i inferred from Doppler spectroscopy vs time corresponding to cases (a)–(h) of Table I (shot ranges 1594–1625, 1744–1776, 2606–2619, 2307–2346, 1563–1593, 1717–1743, 2139–2168, and 2271–2306, respectively). Error bars indicate $\pm 1\sigma$ variation across approximately five shots per data point (where available). Horizontal dotted lines denote peak T_i based on Eq. (2). Dotted lines overlaying the data are ion-electron temperature relaxation based on Eq. (3). Stars indicate peak T_i from 1D-equivalent multifluid simulations (see text; star positions are not intended to reflect the simulation time). The $T_e \lesssim 3$ eV in all cases (see Table I).

radiative losses and tabular EOS, of peak T_i (stars in Fig. 4) using the CHICAGO code [43,44]. For collisional cases [Figs. 4(a)–4(c) and 4(g)], the calculated peak-T_i values are lower than Eq. (2) (as expected with inclusion of thermal or radiative losses) but are also somewhat lower than the data. For interpenetrating cases [Figs. 4(d)–4(f) and 4(h)], the calculated peak-T_i values agree reasonably well with the data. Remaining discrepancies motivate detailed, multidimensional validation studies beyond the scope of this work.

In conclusion, we report a comprehensive experimental study of ion heating in collisional plasma shocks and interpenetrating supersonic plasma flows formed by the oblique merging of two laboratory plasma jets. The post-merge $T_i \gg T_e$ in all cases investigated, including for both very small and substantial jet interpenetration, indicating that the predominant heating goes to the ions for both cases. For cases with shock formation, the measured peak T_i

agrees in most cases with the theoretically predicted T_i jump for a collisional plasma shock [Eq. (2)]. For interpenetrating cases, the measured peak T_i, unsurprisingly, is substantially below that predicted by collisional plasma-shock theory. The predicted classical ion-electron temperature relaxation compares reasonably well with the observed T_i decay. Multifluid CHICAGO simulations show some agreement with the peak-T_i data in both the shock-forming and interpenetrating cases; the differences highlight an opportunity for detailed, multidimensional model validation for this and other codes being used to design and advance our understanding of HED and ICF experiments.

We acknowledge J. Dunn, E. Cruz, A. Case, F. D. Witherspoon, S. Brockington, J. Cassibry, R. Samulyak, P. Stoltz, Y. C. F. Thio, and D. Welch for technical support and/or useful discussions. This work was supported by the Office of Fusion Energy Sciences and the Advanced Research Projects Agency–Energy of the U.S. Dept. of Energy under Contract No. DE-AC52-06NA25396.

[*]samuel.langendorf@lanl.gov
[†]scotthsu@lanl.gov

[1] R. Blandford and D. Eichler, Phys. Rep. **154**, 1 (1987).
[2] A. Bell, Mon. Not. R. Astron. Soc. **182**, 147 (1978).
[3] D. Ryu, H. Kang, E. Hallman, and T. Jones, Astrophys. J. **593**, 599 (2003).
[4] M. Markevitch, A. Gonzalez, L. David, A. Vikhlinin, S. Murray, W. Forman, C. Jones, and W. Tucker, Astrophys. J. Lett. **567**, L27 (2002).
[5] R. P. Drake, *High-Energy-Density Physics* (Springer, Berlin, 2006).
[6] S. Atzeni and J. Meyer-ter-Vehn, *The Physics of Inertial Fusion* (Oxford University Press, New York, 2004).
[7] J. D. Jukes, J. Fluid Mech. **3**, 275 (1957).
[8] M. Y. Jaffrin and R. F. Probstein, Phys. Fluids **7**, 1658 (1964).
[9] E. S. Weibel, Phys. Rev. Lett. **2**, 83 (1959).
[10] W. Fox, G. Fiksel, A. Bhattacharjee, P.-Y. Chang, K. Germaschewski, S. X. Hu, and P. M. Nilson, Phys. Rev. Lett. **111**, 225002 (2013).
[11] C. M. Huntington *et al.*, Nat. Phys. **11**, 173 (2015).
[12] D. A. Tidman and N. A. Krall, *Shock Waves in Collisionless Plasmas* (Wiley, New York, 1971).
[13] E. C. Merritt, A. L. Moser, S. C. Hsu, J. Loverich, and M. Gilmore, Phys. Rev. Lett. **111**, 085003 (2013).
[14] E. C. Merritt, A. L. Moser, S. C. Hsu, C. S. Adams, J. P. Dunn, A. Miguel Holgado, and M. A. Gilmore, Phys. Plasmas **21**, 055703 (2014).
[15] A. L. Moser and S. C. Hsu, Phys. Plasmas **22**, 055707 (2015).
[16] A. J. Harvey-Thompson, S. V. Lebedev, S. Patankar, S. N. Bland, G. Burdiak, J. P. Chittenden, A. Colaitis, P. De Grouchy, H. W. Doyle, G. N. Hall, E. Khoory, M. Hohenberger, L. Pickworth, F. Suzuki-Vidal, R. A. Smith, J. Skidmore, L. Suttle, and G. F. Swadling, Phys. Rev. Lett. **108**, 145002 (2012).
[17] G. Swadling, S. Lebedev, N. Niasse, J. Chittenden, G. Hall, F. Suzuki-Vidal, G. Burdiak, A. Harvey-Thompson, S. Bland, P. De Grouchy, E. Khoory, L. Pickworth, J. Skidmore, and L. Suttle, Phys. Plasmas **20**, 022705 (2013).
[18] G. F. Swadling, S. V. Lebedev, A. J. Harvey-Thompson, W. Rozmus, G. C. Burdiak, L. Suttle, S. Patankar, R. A. Smith, M. Bennett, G. N. Hall, F. Suzuki-Vidal, and J. Yuan, Phys. Rev. Lett. **113**, 035003 (2014).
[19] H. G. Rinderknecht, H.-S. Park, J. S. Ross, P. A. Amendt, D. P. Higginson, S. C. Wilks, D. Haberberger, J. Katz, D. H. Froula, N. M. Hoffman, G. Kagan, B. D. Keenan, and E. L. Vold, Phys. Rev. Lett. **120**, 095001 (2018).
[20] L. Romagnani, S. V. Bulanov, M. Borghesi, P. Audebert, J. C. Gauthier, K. Lowenbruck, A. J. Mackinnon, P. Patel, G. Pretzler, T. Toncian, and O. Willi, Phys. Rev. Lett. **101**, 025004 (2008).
[21] Y. Kuramitsu, Y. Sakawa, T. Morita, C. D. Gregory, J. N. Waugh, S. Dono, H. Aoki, H. Tanji, M. Koenig, N. Woolsey, and H. Takabe, Phys. Rev. Lett. **106**, 175002 (2011).
[22] D. D. Ryutov, N. L. Kugland, H.-S. Park, C. Plechaty, B. A. Remington, and J. S. Ross, Phys. Plasmas **19**, 074501 (2012).
[23] J. S. Ross *et al.*, Phys. Plasmas **19**, 056501 (2012).
[24] J. S. Ross *et al.*, Phys. Rev. Lett. **118**, 185003 (2017).
[25] P. T. Rumsby, J. W. M. Paul, and M. M. Masoud, Plasma Phys. **16**, 969 (1974).
[26] S. M. Pollaine, R. L. Berger, and C. J. Keane, Phys. Fluids B **4**, 989 (1992).
[27] A. S. Wan, T. W. Barbee, R. Cauble, P. Celliers, L. B. Da Silva, J. C. Moreno, P. W. Rambo, G. F. Stone, J. E. Trebes, and F. Weber, Phys. Rev. E **55**, 6293 (1997).
[28] M. Casanova, O. Larroche, and J.-P. Matte, Phys. Rev. Lett. **67**, 2143 (1991).
[29] R. L. Berger, J. R. Albritton, C. J. Randall, E. A. Williams, W. L. Kruer, A. B. Langdon, and C. J. Hanna, Phys. Fluids B **3**, 3 (1991).
[30] F. Vidal, J. P. Matte, M. Casanova, and O. Larroche, Phys. Fluids B **5**, 3182 (1993).
[31] B. D. Keenan, A. N. Simakov, L. Chacon, and W. T. Taitano, Phys. Rev. E **96**, 053203 (2017).
[32] B. D. Keenan, A. N. Simakov, W. T. Taitano, and L. Chacon, Phys. Plasmas **25**, 032103 (2018).
[33] S. C. Hsu, A. L. Moser, E. C. Merritt, C. S. Adams, J. P. Dunn, S. Brockington, A. Case, M. Gilmore, A. G. Lynn, S. J. Messer, and F. D. Witherspoon, J. Plasma Phys. **81**, 345810201 (2015).
[34] S. C. Hsu, S. J. Langendorf, K. C. Yates, J. P. Dunn, S. Brockington, A. Case, E. Cruz, F. D. Witherspoon, M. A. Gilmore, J. T. Cassibry, R. Samulyak, P. Stoltz, K. Schillo, W. Shih, K. Beckwith, and Y. C. F. Thio, IEEE Trans. Plasma Sci. **46**, 1951 (2018).
[35] F. D. Witherspoon, S. Brockington, A. Case, E. Cruz, M. Luna, and Y. C. F. Thio, Bull. Am. Phys. Soc. **62**, 324 (2017).
[36] S. C. Hsu, E. C. Merritt, A. L. Moser, T. J. Awe, S. J. E. Brockington, J. S. Davis, C. S. Adams, A. Case, J. T. Cassibry, J. P. Dunn, M. A. Gilmore, A. G. Lynn, S. J. Messer, and F. D. Witherspoon, Phys. Plasmas **19**, 123514 (2012).
[37] E. C. Merritt, A. G. Lynn, M. A. Gilmore, and S. C. Hsu, Rev. Sci. Instrum. **83**, 033506 (2012).

[38] J. J. MacFarlane, I. E. Golovkin, P. R. Woodruff, D. R. Welch, B. V. Oliver, T. A. Mehlhorn, and R. B. Campbell, in *Inertal Fuion Sciences and Appliations 2003*, edited by B. A. Hammel, D. D. Meyerhofer, and J. Meyer-ter-Vehn (American Nuclear Society, LaGrange Park, IL, 2004), p. 457.

[39] J. D. Huba, *NRL Plasma Formulary* (U.S. Naval Research Laboratory, Washington, DC, 2016).

[40] S. Messer, A. Case, L. Wu, S. Brockington, and F. D. Witherspoon, Phys. Plasmas **20**, 032306 (2013).

[41] See Supplemental Material at http://link.aps.org/supplemental/10.1103/PhysRevLett.121.185001 for derivation of Eq. (2).

[42] H. W. Liepmann and A. Roshko, *Elements of Gasdynamics* (Wiley, New York, 1957), p. 60.

[43] C. Thoma, D. R. Welch, R. E. Clark, N. Bruner, J. J. MacFarlane, and I. E. Golovkin, Phys. Plasmas **18**, 103507 (2011).

[44] C. Thoma, D. Welch, R. Clark, D. Rose, and I. Golovkin, Phys. Plasmas **24**, 062707 (2017).